


Dependence of Two-Photon eGFP Bleaching on Femtosecond Pulse Spectral Amplitude and Phase

David J. L. Graham^{1,2}  · Shu-Fen Tseng^{1,2} · Jer-Tsong Hsieh² · David J. Chen² · George Alexandrakis^{1,2}

Received: 13 June 2015 / Accepted: 14 September 2015 / Published online: 28 September 2015
© Springer Science+Business Media New York 2015

Abstract Photobleaching is a key limitation in two-photon imaging of fluorescent proteins with femtosecond pulsed excitation. We present measurements of the dependence of eGFP photobleaching on the spectral amplitude and phase of the pulses used. A strong dependence on the excitation wavelength was confirmed and measured over a 800–950 nm range. A fiber continuum light source and pulse shaping techniques were used to investigate photobleaching with broadband, 15 fs transform limited, pulses with differing spectral amplitude and phase. Narrow band pulses, > 150 fs transform limited, typical of femtosecond laser sources used in two-photon imaging applications, were also investigated for their photobleaching dependence on pulse dispersion and bandwidth. The bleach rate for broadband pulses was found to be primarily determined by the second harmonic spectrum of the excitation light. On the other hand, for narrow band excitation pulses with similar center wavelengths improvement in bleach rate was found to be mostly dependent on reducing the pulse length. A simple model to predict the relative bleach rates for broadband pulses is presented and compared to the experimental data.

Keywords Two-photon · eGFP · Pulse shaping · Photobleaching · Fiber continuum

Introduction

Two-photon laser scanning microscopy enables depth resolved imaging of fluorescent samples at sub-micron spatial resolution through tissues [1]. The reduced scattering of near-infrared excitation light by biological tissues, relative to visible or UV one photon excitation, allows imaging at depths of up to ~1 mm [2], or deeper if longer wavelength near-infrared femtosecond pulse sources are available [3]. Though originally applied to dyes [4] the development of fusion proteins, where a fluorescent label is tagged to the C- or N-terminus of an existing protein, has enabled the use of two-photon excitation for monitoring protein expression and kinetics [5]. Many fusion protein tag colors have been developed [6–8] but the green fluorescent protein, originally derived from the jellyfish *Aequorea victoria*, was the first to be cloned and its eGFP variant [9] remains an important tool in biology today.

Photobleaching is a key limitation in two-photon imaging of fluorescent proteins. The excitation power must be limited to maintain an acceptable bleach rate, which may compromise the signal-to-noise ratio (SNR). This is a particularly severe problem in quantitative measurements e.g. fluorescence correlation spectroscopy [10, 11] or raster imaging correlation spectroscopy [12], where a high SNR is necessary for meaningful results. Chemical agents can improve bleaching [13] but are inconvenient or impossible to use in live samples.

Changing the properties of the light used for two-photon excitation can reduce bleaching. Simply changing from a

This work was supported in part by the National Cancer Institute [5R21CA154958-02] and the Cancer Prevention and Research Institute of Texas [RP110465-P1, RP110465-C2].

✉ David J. L. Graham
davgrah@uta.edu

¹ Bioengineering Department, University of Texas at Arlington, Arlington, TX 76019, USA

² University of Texas Southwestern Medical Center, 5323 Harry Hines Boulevard, Dallas, TX 75390, USA

850 nm to 920 nm center excitation wavelength has been shown to reduce the bleaching of enhanced green fluorescent protein (eGFP) by a factor of two at constant excitation power [14]. Using a lower repetition rate relative to the ~ 80 MHz of standard pulsed sources has also been shown to reduce bleaching [15], by allowing dark state relaxation. Interestingly, using a higher repetition rate has also been shown to give an improvement [16], possibly due to the reduced peak power used. Using pulse shaping techniques a significant reduction in the bleaching of a fluorescence standard has been demonstrated for 10 fs transform limited (TL) pulses compared to dispersion broadened ones [17]. Improved bleaching has also been observed by reducing pulse duration for red fluorescent protein (RFP) and rhodamine B [18] with ~ 50 fs TL pulses versus dispersion broadened ones. For eGFP transform limited pulses may not be optimal as Kawano et al. [19] demonstrated four-fold reduction in bleaching with a phase modulated pulse versus a TL one.

The above reports suggest that current knowledge on the femtosecond pulse parameters affecting eGFP bleaching is fragmentary. This has motivated us to perform a systematic study of the eGFP bleaching dependence on femtosecond pulse spectral content and phase profiles so as to suggest possible optimal pulse parameters to other investigators performing two-photon imaging with eGFP. In this paper we present measurements of eGFP bleaching for excitation pulses of varying wavelength content and shape. The wavelength dependence of eGFP two-photon bleaching was measured over a 800–950 nm wavelength range that covers most of its excitation spectrum that is accessible by standard Ti:Sapphire lasers. We confirmed that the bleach rate is strongly influenced by the excitation wavelength with an order of magnitude decrease between 800 nm and 950 nm for the same excitation rate. Changes in bleaching for different pulse shapes were investigated with a fiber continuum light source and a phase and amplitude pulse shaper. For broadband (~ 15 fs transform limit) pulses large changes in bleach rate could be obtained by phase or amplitude shaping. To explain the broadband pulse results we present a simple model using the data from our measurements of bleaching as a function of excitation wavelength. It is shown that the main cause of differences in bleaching rate is the differences in the second harmonic spectra of the pulses. For pulse shaping measurements with a narrower bandwidth of ≈ 165 fs TL, more typical for two-photon microscopy, measurements without the fiber source allowed higher bleaching rate measurement accuracy. A small improvement in bleaching for pulses compressed to the transform limit versus dispersion-broadened pulses was found that is not caused by differences in the second harmonic spectrum composition.

Materials and Methods

Preparation of eGFP

The eGFP used for this work was produced in BL21 codon plus competent *Escherichia coli* (*E. coli*) cells (Agilent Technologies, Santa Clara, CA). To prepare the pQE80-EGFP vector used the EGFP coding sequence was amplified by PCR using pEGFP-c1 (Addgene, Cambridge, MA) as a template. Primers used were forward primer, 5-GC-GAGATCTGTGAGCAAGGGCGAGGAGCTG-3 and reverse primer, 5-GCGGGATCCCTTGTACAGCTCGTC-CATGCC-3. The PCR product, purified from agarose gel, was inserted into pQE80L (Addgene) by Bgl II and BamH I DNA restriction enzymes (Life technologies, Thermo Fisher Scientific, Waltham, MA). *E. coli* cells were transformed with pQE80-EGFP and grown in 3 ml LB broth containing Ampicillin ($50 \mu\text{g/ml}$), at 37°C and 350 rpm overnight. 1.5 ml of the resulting culture was transferred to 260 ml of fresh LB broth containing Ampicillin, and grown until an OD_{600} of 0.5 was reached. The cells were then incubated with 1 mM Isopropyl β -D-1thiogalactopyranoside (IPTG) at 30°C and 150 rpm for 6.5 hours. Cells were centrifuged at $9000 g$ and 4°C for 15 min and the resulting cell pellets lysed using TALON® xTractor buffer (Clontech, Mountain View, Ca) with 1 mM phenylmethanesulfonyl fluoride (PMSF) at 4°C for 15 min. The supernatant was then obtained by centrifugation at $10000 g$ and 4°C for 20 min, and filtered with a $0.22 \mu\text{m}$ filter. The eGFP protein was purified using a HisTALON Gravity column purification Kit (Clontech) according to the instructions of the manufacturer and then concentrated by ultrafiltration using a Centricon 50 filter (Ambion, Life technologies). Aliquots of the protein diluted to $40 \mu\text{M}$ in 20 mM Tris buffer (pH 7.4), containing 1 mM PMSF (phenylmethanesulfonyl fluoride), $200 \mu\text{M}$ sodium orthovanadate (Na_3VO_4), and 10 mM Sodium Fluoride were frozen at -80°C in plastic tubes for long-term storage.

Experimental Apparatus

Three different experimental systems were used for the work presented in this paper. As all three are similar the system used for measuring photobleaching as a function of excitation wavelength will be described in detail and then the two pulse shaping systems used described as variations of the first system. A schematic of the experimental setup used for the bleaching versus wavelength measurements is shown in Fig. 1a, beam path 1. A Ti:Sapphire laser (Mai Tai HP, Santa Clara, CA) was used as a source of ~ 150 fs NIR pulses with a 80 MHz repetition

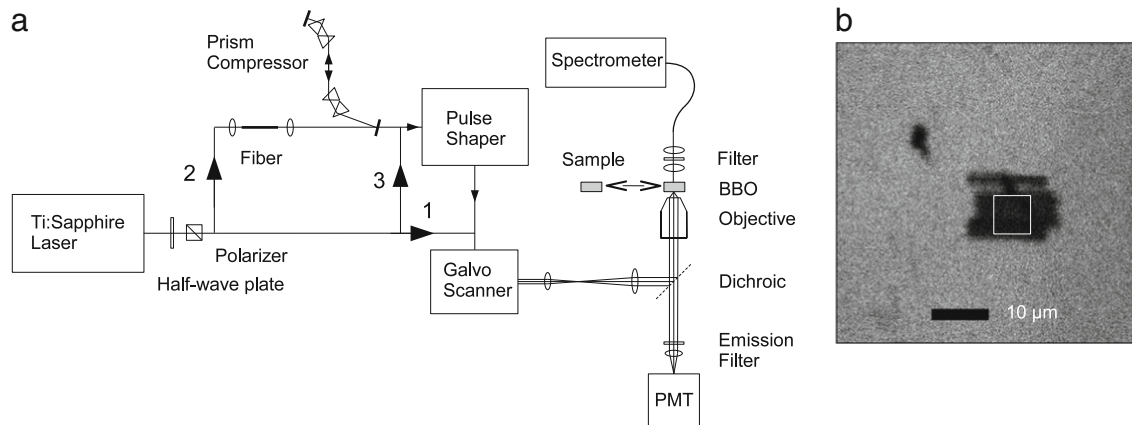


Fig. 1 (a) The two-photon fluorescence microscope. PMT: photon counting photomultiplier, BBO: β Barium Borate second harmonic generation crystal that can be exchanged with the fluorescent sample. Three different setups with beam paths 1, 2 and 3 are used for measurement of bleaching as a function of wavelength, pulse shape with

broadband pulses and pulse shape with narrow band pulses, respectively. (b) Example bleached area on an eGFP-coated surface. Data from the indicated square area was used to calculate the bleaching rate induced by different spectral content and phase profile femtosecond pulses

rate.¹ Beam power was controlled by a half-wave plate followed by a Glan-Laser polarizer. Protected gold surface mirrors in kinematic mounts were used to steer the beam to the microscope and a 2-axis Galvo mirror scanner with controller (A402 and A403, ISS Inc, Champaign, IL) was used to raster scan images. A dichroic mirror directed the beam into the side port of an inverted microscope (Axio Observer Z1, Zeiss, Oberkochen, Germany). A 100 mm achromat scanning lens (Thorlabs, Newton, NJ) was used in combination with the microscope's 200 mm tube lens to create an expanded and collimated ~ 4 mm FWHM beam at the objective's back aperture. The 0.75 numerical aperture (NA) 40 \times objective (EC Plan-Neofluar, Zeiss) was under-filled by the beam to give a 0.5 NA focus. This lower numerical aperture made the system less sensitive to focus errors and the excitation power could be increased to give the same intensity at the focus as for a typical ~ 1 NA two-photon system. Sample fluorescence collected by the objective was transmitted through the dichroic and focused on a photon counting photomultiplier (H7421-40, Hamamatsu, Shizuoka, Japan). A bandpass filter (ET525/50, Chroma, Bellows Falls, VT) was used to remove background and scattered excitation light. A 1 OD neutral density filter (ND10A, Thorlabs) was also used to reduce the count rate allowing higher concentrations of eGFP that were more easily measured, as at concentrations below ~ 1 nM adhesion of eGFP to plastic pipettes and mixing tubes occurred for a significant population fraction of the fluorophore.

Samples were contained in 800 μ L well plates with a #1 cover-glass base (No 155411, Thermo Fisher Scientific). For bleaching measurements eGFP was deposited on the well plate cover-glass surface and a small area was imaged continuously. During the experiments eGFP was stored at -20 $^{\circ}$ C with single samples defrosted as needed and refrigerated for no more than 3 days. A portion of the eGFP solution was diluted to 20 nM with phosphate buffered saline (PBS, Sigma-Aldrich, St. Louis, MO), and 600 μ L were immediately added to a well chamber. The solution was stirred with a pipette, then covered and left for 30 minutes to ensure that the eGFP had completely adhered to the cover-glass.

Additional optics were used to allow simple focusing and excitation power monitoring. An uncoated BK7 4 $^{\circ}$ wedge prism (Thorlabs) was placed in the beam path shortly before it entered the scanner. The power reflected from the prism was calibrated to the power at the focus by removing the objective, placing a power meter (PS10, Coherent, Santa Clara, CA) on the microscope stage and then factoring in the loss through the objective as specified by the manufacturer. Light back-scattered from the sample and reflected from the prism was focused on a 50 μ m pinhole with a 200 mm achromat (Thorlabs) and detected with a photodiode (PDA36A, Thorlabs). The microscope focus was adjusted for maximum photodiode signal which focused the excitation light on the cover glass surface with an accuracy of ± 0.1 μ m.

The microscope was controlled by ISS VistaVision software running on a Windows XP PC with an 3-axis DaQ Board (v1.1, ISS) and board detector (v1.0, ISS). After focusing on the glass surface 64 \times 64 pixel images were

¹This laser is rated to produce 100 fs pulses but the one used was old and in need of adjustment.

taken of a $10 \times 10 \mu\text{m}$ area with $40 \mu\text{s}$ integration per pixel. The pixel size was much smaller than the point spread function so that eGFP located on and in-between scan lines was bleached equally. Typically 100 frames were recorded with more taken if needed to ensure that the brightness had reduced to less than $1/2$ of its original value. Figure 1b shows an image of the eGFP-coated surface after a typical measurement. The area bleached by the scan and a spot bleached when focusing are clearly visible.

To analyze the results, first the center 45×45 pixels of each frame were averaged to improve the statistics. A double exponential decay, $A_1 e^{-\alpha} + A_2 e^{-\beta}$, least mean squares fit (*lsqcurvefit* function, MATLAB) was made to the average count rate versus frame number so as to determine the number of frames needed to attain 50 % bleaching relative to the original brightness.

To calibrate excitation power to the relative rate of eGFP excitation, brightness measurements were performed in solution. Brightness measurements used a 200 nM eGFP solution in PBS (Sigma-Aldrich), with 0.5 % bovine serum albumin (BSA, BP1600-100, Thermo Fisher Scientific) to prevent the protein from sticking to the cover-glass. This was imaged with the same parameters as the bleaching measurements except that the objective was focused $20 \mu\text{m}$ from the cover-glass. This avoided the influence of any eGFP that persisted adhering to the glass despite non-specific binding blockage by BSA. The brightness was recorded as the average photon count rate for the center 45×45 pixels averaged over 20 frames. For the range of powers and wavelengths used no saturation was observed and the brightness was proportional to the square of the excitation power. This allowed one brightness measurement per wavelength to be scaled to different excitation powers. All brightness measurements could then be completed in 30 minutes thus avoiding errors due to sample decay or mixing different samples.

Fiber Source Apparatus

Measurements of the dependence of eGFP bleaching on pulse spectral amplitude and phase were made using a spatial light modulator (SLM) based pulse shaper combined with a fiber continuum light source. The apparatus was similar to the bleaching versus wavelength system described above so only the differences and new components are described here; see Fig. 1a for the system layout using beam path 2. The Zeiss microscope body was not used for these measurements due to its poor transmission beyond 900 nm and high dispersion. Instead, the microscope sample stage and objective were mounted separately with a 200 mm achromat tube lens. A different Ti:Sapphire laser (Chameleon Ultra, Coherent, Santa Clara, CA) was used to pump the fiber light source. This laser was originally

intended to be used for all measurements presented in this work but it failed after completion of the fiber source measurements. The differences between the two lasers are not important as this laser was only used with the fiber and pulse shaper where the laser output was drastically modified and then characterized.

Broadband pulses were created by continuum generation in a highly nonlinear optical fiber [20]. The fiber used is the NL-1050-NEG-1 Nonlinear Photonic Crystal Fiber (NKT Photonics, Birkerød, Denmark). This is a silica fiber with a $2.3 \pm 0.3 \mu\text{m}$ core at the center of a hexagonal array of air holes that has been previously characterized for continuum generation [21]. Due to its all-normal group velocity dispersion this fiber broadens the excitation pulse spectrum by self-phase modulation and optical wave breaking [22] with less sensitivity to the input pulse properties and a more coherent output compared to anomalous group velocity dispersion fibers [20, 23].

A 20 mm piece of the fiber was cut, the air holes of the microstructure were collapsed with a fusion splicer and then cleaved about $100 \mu\text{m}$ from the start of the uncollapsed microstructure. This length was chosen as short enough to allow a high power throughput without the spectrum becoming broader than desired and not too short for easy handling. The fiber was mounted in a clamp on a 3-axis flexure stage (MAX312D, Thorlabs), the beam was coupled to it with an aspheric lens (C392TME-B, Thorlabs) and its output was subsequently collimated with a microscope objective (M-20X, Newport, Irvine, CA). A Faraday rotator was placed between laser and fiber to reduce the effect of back reflections. A double prism compressor [24] using four fused silica Brewster prisms (10SB10, Newport) and a gold coated folding mirror (Newport) applied $\sim 5000 \text{ fs}^2$ of dispersion compensation. This gave approximately zero second order dispersion at the sample so that the limited range of applied spectral phase from the pulse shaper was only needed to compensate higher order dispersion.

A femtosecond pulse shaper (femtoJock, BioPhotonic Solutions, East Lansing, MI) was used to control the spectral amplitude and phase. The femtoJock system implemented the multiphoton intrapulse interference phase scan (MIIPS) method [25, 26] that enabled the applied spectral phase for dispersion compensation and pulse compression of the fiber output to be found. Use of the femtoJock system [27] and similar pulse shapers for two photon microscopy has been reported previously [28].

The pulse shaper diffraction grating was adjusted to project the 780–1000 nm range over the 128 SLM pixels, to give a $\sim 2 \text{ nm}$ resolution, and was calibrated in accordance with the manufacturer's instructions. The phase resolution depends on wavelength and applied phase with a typical value near the middle of the range of $\sim 3^\circ$. The pulse shaper's supplied polarizer was mounted into the beam

path after the shaper and tilted slightly to split some back-reflected light from the sample for focusing the objective on the sample as done for the wedge prism used previously for the bleaching versus wavelength measurements. For the analysis presented and for MIIPS pulse compression the second harmonic spectrum of the beam must be measured. The 10 μm β barium borate (BBO) crystal with glass backing supplied with the femtoJock was mounted on a cover slip and placed in the sample position. Two achromat lenses focused the second harmonic light into a fiber-coupled spectrometer (USB 4000, Ocean Optics, Dunedin, FL) with the fundamental blocked by a colored glass filter (FGS900, Thorlabs). Spectra were corrected for the wavelength sensitivity of the spectrometer sensor given in its data sheet. The spectrometer was also used to measure the fundamental spectrum by placing its input fiber directly in front of the objective.

The laser was set to a 870 nm center wavelength (pulse length ~ 200 fs) and the input power to the fiber was 330 mW to give a 135 mW output spectrum spanning 150 nm. The MIIPS software was set to compress the pulse using six iterations, one cubic and then five sinusoidal phase corrections, with the best compression found on the fifth iteration.² Intensity as a function of time, $I(t)$, could be calculated numerically from the fundamental spectrum and the residual phase after compression found by the MIIPS software. For each time point 10000 complex phasors with frequencies linearly spaced over the wavelength range, and the measured spectral amplitudes and phases, were added. The intensity envelope was then found from the absolute value squared. This gave a 15 fs pulse length FWHM for the compressed pulse. The second order temporal coherence $g = \langle I^2(t) \rangle / \langle I(t) \rangle^2$ [4] which relates the intensity of two-photon effects to the intensity of the fundamental could also be calculated from $I(t)$ after taking into account the 80 MHz repetition rate.

The high sensitivity of beam coupling to the small core fiber on small drifts and vibration in addition to variations in the laser output caused fluctuations in the output spectrum. To mitigate the effects of the resulting pulse output variability on bleach time determination all bleaching measurements were performed three times and their bleach times were averaged.

Narrow Band Pulse Shaping

The pulse shaper was also used without the fiber source to investigate the effect of dispersion for pulses with a narrower spectral bandwidth more typical of pulsed sources

used in two-photon microscopy. The apparatus was the same as for the bleaching versus wavelength measurement except that the beam from the Mai Tai laser was diverted through the pulse shaper as shown in Fig. 1a, beam path 3. The laser was set to 920 nm, near the eGFP excitation peak [8], with a bandwidth of 6.3 nm FWHM and TL pulse length ≈ 165 fs. The diffraction grating in the pulse shaper was replaced with one which gave a resolution of 0.4 nm per channel and the system was re-calibrated. The second harmonic detection components used with the fiber source could be mounted on the microscope sample stage. MIIPS pulse compression was performed as described above as were the pulse length and g calculations from the measured data.

Results and Discussion

Bleaching Rate versus Wavelength

To provide data for the analysis of the bleaching measurements with broadband pulses, we measured bleach rate as a function of excitation wavelength for a 800 – 950 nm wavelength range in 10 nm steps that covered most of the eGFP excitation peak. The measured center wavelength typically differed by a few nm from the value selected with the laser control software so the measurements were not at uniformly spaced wavelengths. The mean bandwidth of the laser output in the measurement range was 7 nm FWHM, standard deviation 1 nm. For each center wavelength the selected excitation power was varied to attain 50 % fluorescence intensity reduction after 2 to 80 scanning frames. Data for 860 nm is omitted as the laser was unstable at this wavelength and results were inconsistent. The brightness and thus relative excitation rate was measured for each selected wavelength using the eGFP BSA solution described in the Methods.

A clear dependence of bleaching on wavelength was found with shorter excitation wavelengths having greatly increased bleaching, consistent with a previous report [14]. For example changing the laser setting from 820 to 940 nm (824 and 947 nm measured center wavelength) reduced the bleach rate by almost a factor of 10 for equal excitation rates as shown in Fig. 2a.

A two-dimensional surface was fitted to the measured eGFP bleaching rate data to allow estimation of bleaching rate for any brightness and excitation wavelength within the explored parameter range. The function fitted by least mean squares over 106 distinct measurement points between 800 nm and 950 nm (Fig. 2b) was

$$\log B_r = a + b\lambda + c\lambda^2 + d \log B, \quad (1)$$

with $a = 55.3$, $b = -0.138$, $c = 7.42 \times 10^{-5}$, $d = 1.67$, where λ was wavelength, B the brightness (counts per

²After the MIIPS algorithm reaches a nearly transform limited pulse it is noise limited and subsequent iterations are not necessarily improvements.

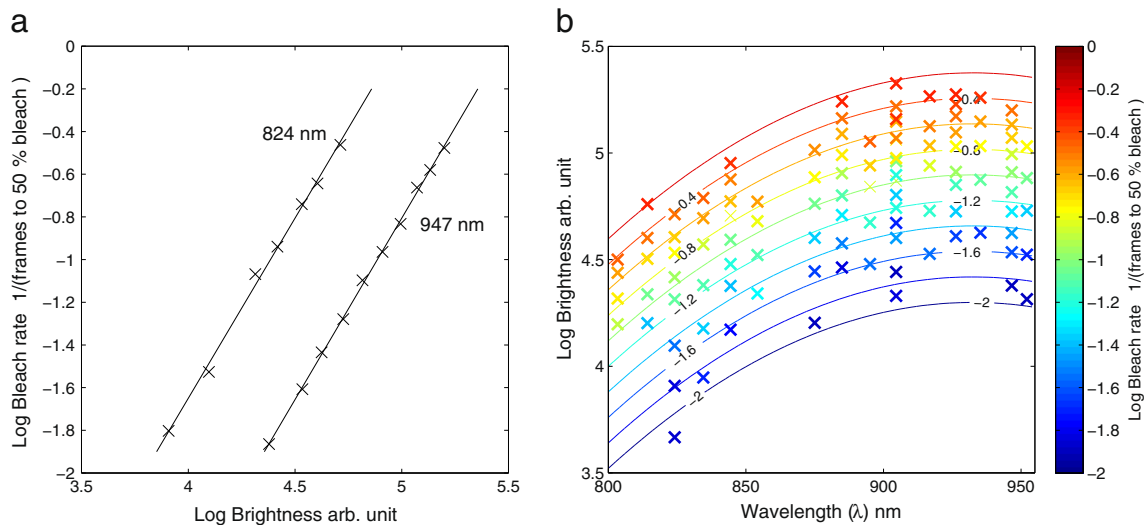


Fig. 2 (a) A log–log plot of bleach rate versus brightness for two example wavelengths. Excitation power range was 8.4–21.3 mW for 824 nm and 9.2–23.7 mW for 947 nm. Slope of fitted lines is 1.69 for 824 nm and 1.70 for 947 nm. (b) Magnitude of log bleach rate

second) and B_r , the bleach rate (1/ frames to 50 % bleach). These fitted parameters gave $R^2 = 0.94$. Assuming a linear wavelength dependence between $\log(B_r)$ and $\log B$ gave a poorer fit ($R^2 = 0.87$) while addition of a cubic term gave no improvement ($R^2 = 0.94$) relative to the quadratic. The fitted bleaching rate versus wavelength function was used for analysis of the pulse shaper measurements presented here below.

The eGFP Bleaching Rate from Broadband Pulses

To analyze the dependence of photobleaching on broadband pulse properties the output of the continuum fiber source was directed at the MIIPS pulse shaper and measurements were made using different SLM settings to achieve a variety of distinct pulse spectral amplitudes and phases. As the second harmonic results from the interference of wavelength components of the fundamental spectrum [29], changes in the spectral phase can drastically modify the second harmonic spectrum [30]. Figure 3 shows the spectral and phase properties for each of the 13 pulses generated and studied for their bleach rate in this work. As described in Section 2 the second harmonic spectra were measured with the BBO crystal and spectrometer. The fundamental spectra were measured by removing the sample with the spectrometer input fiber placed in front of the objective. The spectral phase shown is the applied phase selected in the pulse shaper control software, plus the residual phase after compression found by the MIIPS algorithm.

The pulse shaper transmission was adjusted to reduce the excitation power from the 21 mW of maximum output power available and give similar brightness for the eGFP

as a function of eGFP brightness and excitation center wavelength. Points represent bleach rate measurements and contour curves the fitted function (log bleach rate color scale shown on right)

BSA solution for each pulse type. Creating a new transmission profile for the pulse shaper was a slow process so the adjustments were made one hour before the bleaching measurements resulting in some variation in the average brightness attained for each pulse type as in the fiber output drifted.

Pulse 1 (excitation power 2.3 mW) was the full fiber output spectrum with the phase compensation found from the MIIPS system to achieve a linear spectral phase and the shortest possible pulse, resulting in a TL FWHM of 15 fs. For pulses 2 (3.0 mW) and 3 (4.6 mW) pulse shaper amplitude control was used to narrow the spectrum, producing TL pulse lengths of ~ 27 fs and ~ 55 fs respectively. As we found in the previous section that bleach rate is strongly influenced by excitation wavelength (Fig. 2) four pulses with different spectral shifts were used to explore this dependence in more detail. In pulse 4 (3.4 mW), spectral component attenuation selected the short wavelengths. Adding dispersion to the long wavelengths selected the short wavelength second harmonic components without changing the fundamental spectrum for pulse 5 (8.0 mW). Similarly, pulse 6 (2.5 mW) and pulse 7 (3.6 mW) had the long wavelength second harmonic components selected by amplitude and phase changes respectively. As dispersion has been shown to influence two-photon bleaching [17] pulses 8 (2.7 mW), 9 (5.1 mW) and 10 (10 mW) were tested with 100, 300 and 1000 fs^2 dispersion applied. At 100 fs^2 the pulse was broadened to ~ 18 fs and the peak of the second harmonic spectrum flattened. By 1000 fs^2 the pulse was spread over 350 fs and the second harmonic spectrum was multi-peaked. Finally the influence of a higher order dispersion term was tested with pulses 11 (4.3 mW), 12 (5.8 mW) and

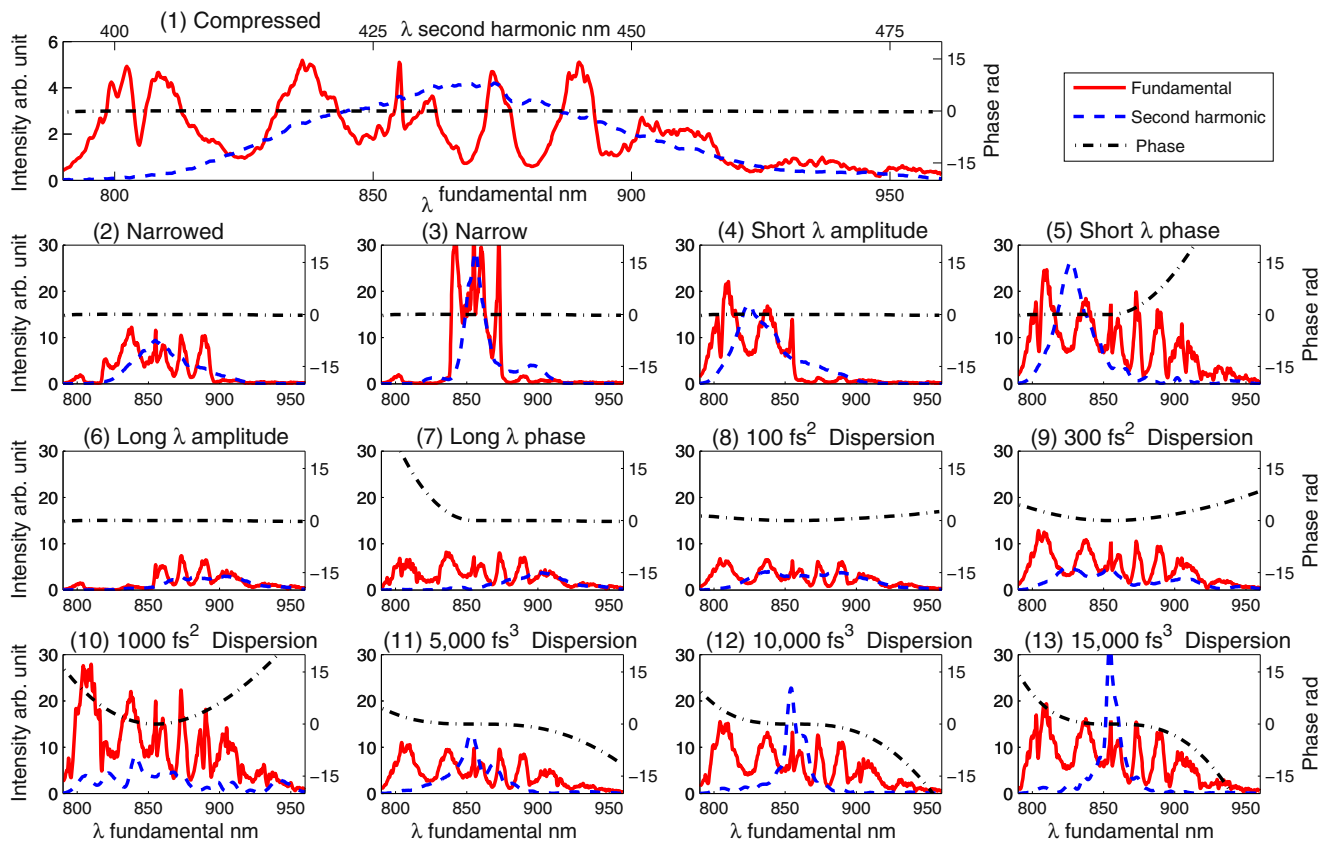


Fig. 3 The 13 different pulse types used to study eGFP bleaching in this work (red curves: excitation wavelength; blue curves: second harmonic; black curves: applied spectral phase; horizontal scale: λ nm, or 2λ nm for the fundamental and second harmonic wavelengths, respectively)

13 (7.5 mW) having 5000, 10000 and 15000 fs^3 third order dispersion. Adding third order dispersion created a narrow bandwidth second harmonic signal without changing the fundamental spectrum [31]. 5000 fs^3 was enough to show significant narrowing while 15000 fs^3 created a single narrow peak in the second harmonic spectrum.

The time to 50 % bleach of eGFP deposited on glass and the brightness of eGFP in solution were measured for each of the above 13 pulse types. Bleaching measurements were repeated three times for each pulse shape and the results were averaged. As there were only three measurements per point the average standard error for all 13 pulses (± 6 frames) was used for each pulse. The main source of this error is expected to have been fluctuations in the fiber source output.

As shown in Fig. 4a the brightness variation for the pulses was clearly not the strongest influence on the bleach time. In contrast, the bleach rate was found to be correlated to excitation wavelength. In Fig. 4b the relative fluorescence yield, equal to the brightness times the time to 50 % bleach, is plotted against the mean excitation wavelength. Most of the pulse shapes followed a clear trend with lower excitation wavelengths producing more rapid bleaching and lower

fluorescence yields. Exceptions to this trend were dispersion broadened pulses 9 and 10, which bleached eGFP more rapidly than other pulse types of similar mean wavelength. These pulses were notable for their broad multi-peaked second harmonic spectra so the mean excitation wavelength may not adequately describe their effect.

We attempted to explain these results using the eGFP bleach rate as a function of excitation wavelength and brightness, B_r , rearranging (1) above as

$$B_r(\lambda) = 10^{((a+b\lambda+c\lambda^2)+d \log B)} \tag{2}$$

with a , b , c , and d parameter values obtained from the fitted data in Fig. 2b.

We hypothesized that the total bleach rate B_{rm} would be related to the bleach rate for each constituent pulse wavelength through linear proportionality to the excitation rate at each wavelength. A weighted average of the predicted bleach rate for each pulse type was then calculated by

$$B_{rm} = \frac{\int B_r(\lambda) I_{shg}(\lambda/2) C_s(\lambda) \cdot d\lambda}{\int I_{shg}(\lambda/2) C_s(\lambda) \cdot d\lambda} \tag{3}$$

where I_{shg} was the measured second harmonic intensity and C_s the two-photon absorption cross-section of eGFP [8],

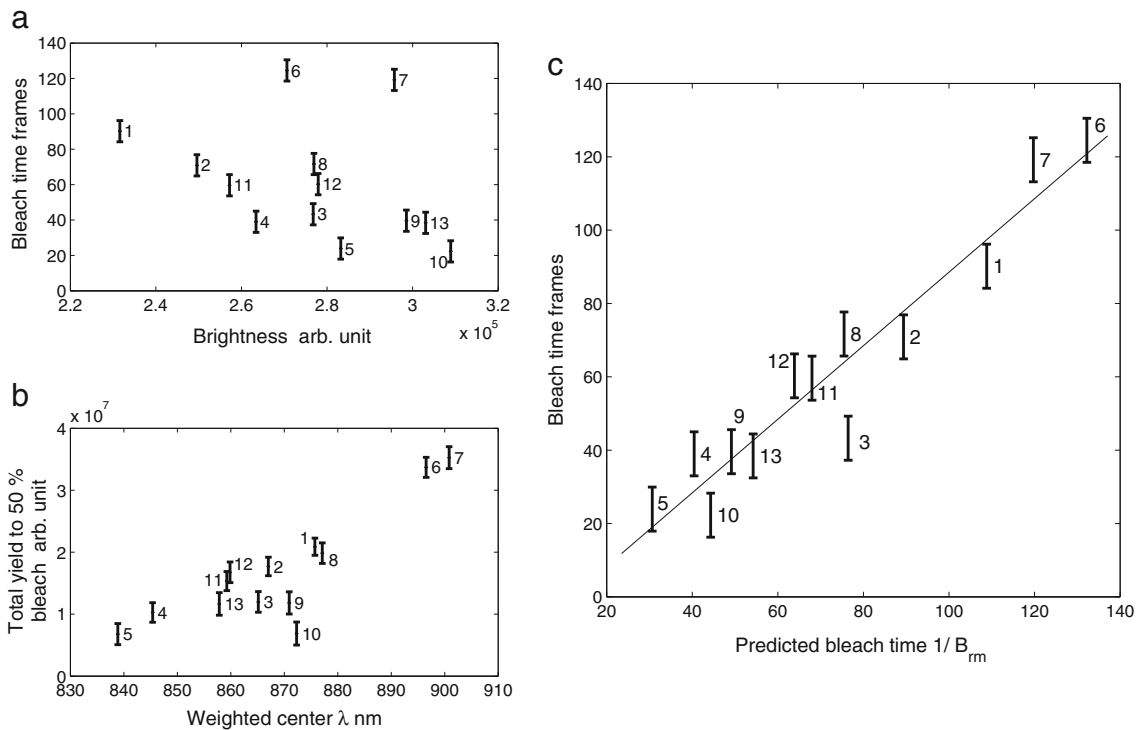


Fig. 4 Bleaching for the fiber source pulse shaping measurements. (a) Bleach time versus (relative) brightness for the 13 pulse shapes. (b) Fluorescence yield versus mean excitation wavelength for the 13 pulse shapes. (c) Measured bleach time versus predicted $1/B_{rm}$. A linear fit

is included to show the correlation between the measured and calculated bleach times ($R^2 = 0.91$). Error bars in all plots are 1σ standard error

with $I_{shg}C_s$ proportional to the excitation rate. The integral was evaluated numerically as a sum over all measured second harmonic wavelengths ($\lambda/2$).

In Fig. 4c the observed bleach time is plotted against $1/B_{rm}$, the expected bleach time. A least mean squares linear fit was made to show the correlation between the predicted and measured bleach times. To calculate the bleach rate B_r for a given wavelength the excitation rate is required. Differences in the setup of the pulse shaper and bleaching versus wavelength measurements make it difficult to directly compare brightness measurements. We therefore used the brightness measured for the 13 different pulse types to calculate the relative excitation rates, which were then multiplied by a single constant adjusted to make the gradient of the linear fit equal to unity. The constant was $C_B = 1.36 \times 10^4$ with the average brightness for the 13 pulses $A_B = 2.76 \times 10^5$ counts per second. As a result for each pulse shape with brightness B_p a brightness of $B = C_B \times B_p/A_B$ was used when calculating B_{rm} .

There was good linear correlation between the expected and measured bleach rates ($R^2 = 0.91$) in Fig. 4c. However there was an offset with all measured times, of approximately 15 frames (or ~ 4 seconds) shorter than expected. This may in part be due to differences in the experimental conditions compared to the wavelength measurements

shown in Fig. 2b. For example the beam diameter and shape at the back aperture of the objective may have been slightly different. The reduced χ^2 of the fit is 3.5 indicating that other factors are influencing the bleaching or the errors have been underestimated. It is suspected that this is mostly due to drift in the fiber source output spectrum over the course of the experiment. Nevertheless, our findings support the hypothesis that the second harmonic component of pulses is the main factor determining the relative bleach rates.

The possibility that the bleaching was influenced directly by the excitation power or second order temporal coherence (g) was considered. The residual of the fit of bleach time versus $1/B_{rm}$ was calculated for all 13 points. If excitation power or g were significantly influencing the bleach rate they would have been correlated with the residual. No significant correlations were observed indicating that any effect is below the noise level.

We then considered if the agreement between measured and calculated bleach rates could be improved by including the effect of reduction in the diffraction limited spot size for the shorter wavelengths. The resulting higher intensity at the focus would increase the strength of two-photon effects at the cover-slip surface. In the eGFP solution or BBO crystal an increase in two-photon effects may not be observed due to the decreased depth of field. No

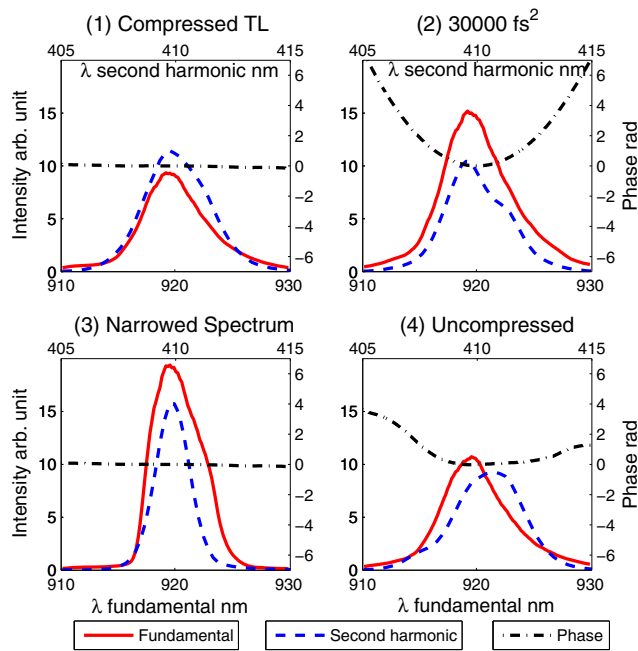


Fig. 5 Spectral phase, second harmonic and fundamental spectra of the narrow band pulses used. The small non-zero phase for (1) and (3) is the residual phase after compression as measured by the MIIPS algorithm. For pulse (3) the limited resolution of the spectrometer shows the fundamental slightly wider than it should be (pulse shaper transmission set to 0 outside 917.1–923.8 nm)

significant improvement in the fit of measured bleach time to the expected time ($1/B_{rm}$) was observed when the second harmonic spectra were scaled by the expected increase at short wavelengths.

The eGFP Bleaching Rate from Narrow Band Pulses

In addition to the broadband pulse bleaching measurements studied in the previous section, measurements were also performed for narrow band shaped pulses. Without the need of using the relatively unstable fiber source to produce these pulses, higher accuracy measurements were possible and the narrow bandwidth meant that differences in bleach rate due to the second harmonic spectra were small.

Four different pulse types were used to study the effects of narrow band spectral content on eGFP bleaching. The second harmonic and fundamental spectra of the pulses measured at the focus are shown in Fig. 5 along with the spectral phase. Pulse (1) was the Ti:Sapphire laser output with dispersion compensation found by a MIIPS measurement to obtain the shortest possible pulse length of ≈ 165 fs. Pulse (2) had 30000 fs^2 dispersion added to triple the pulse length and require a significant power increase to achieve the the same brightness as pulse (1). A longer pulse without dispersion (3) was created by using the pulse shaper amplitude control to select only the center 6.6 nm of the laser spectrum. The width of the spectrum was chosen to be as narrow as possible while still allowing the same brightness as pulse (1) with the available beam power. Pulse (4) was the unaltered laser output with no phase compensation applied and $\sim 10000 \text{ fs}^2$ dispersion from the objective and other optics in the beam path. This made pulse (4) similar to a typical simple two-photon imaging system with no pulse shaper or other dispersion compensation. The transmission of the pulse shaper was adjusted to obtain similar brightness in an eGFP BSA solution for all four pulses.

Properties of the pulses used with brightness and bleach time of eGFP are shown in Table 1, with the reported bleach times representing the average of six measurements. The uncertainty of the bleach time measurements was much smaller than for the fiber source data as the system was much more stable without the fiber. For each pulse type the intensity envelope was calculated numerically from the spectral amplitude and phase over the 910 – 930 nm range. From this the pulse length, τ , FWHM and the second order temporal coherence $g = \langle I^2(t) \rangle / \langle I(t) \rangle^2$ were calculated [4].

Significant differences were seen in the bleach time for similar brightness despite the small differences in the second harmonic spectra shown in Fig. 5. Using Eq. 3 to calculate the expected bleach rates indicates that they should vary by $\sim \pm 1\%$. However, pulse (1) that was compressed to the transform limit shows a clear improvement in bleaching over the other pulses that are broadened in time by dispersion, or due to a narrower spectrum. This result is

Table 1 Narrow band pulse properties and eGFP bleach rate

Pulse	Pulse length FWHM fs	g	Excitation power mW	Brightness arb. unit	Bleach Time frames
(1)	165	5.0×10^4	7.6	5.58	56 ± 2
(2)	572	1.6×10^4	13.3	5.54	36 ± 1
(3)	403	2.2×10^4	12.3	5.61	43 ± 1
(4)	275	3.0×10^4	9.1	5.55	45 ± 2

Pulse length FWHM calculated from spectral amplitude and phase; Calculated second order temporal coherence g ; Excitation power at focus; Brightness of the eGFP solution; Bleaching time, measured as number of frames to 50 % reduction in intensity, with mean and 1σ standard error found from 6 measurements

consistent with reported results for red fluorescent protein (RFP) where bleaching increases for longer pulses with lower g [18]. This effect was probably not seen for broadband pulses due to the increased noise from pulse to pulse variability and the large differences in bleach time due to the second harmonic spectra.

Conclusion

This work filled in information lacking from prior reports on eGFP bleaching properties and presented a simple analytical function fit to systematic measurements that can be used by other investigators to estimate eGFP bleaching rate as a function of wavelength. From 800 nm to 950 nm the bleach rate at constant excitation rate changes by an order of magnitude. Operating near the eGFP two-photon cross section peak at 925 nm can therefore produce a significant improvement in both brightness and bleach rate compared to operating at the same power at shorter wavelengths that are often preferred because more output power is available.

The difference in bleaching for different broadband pulse shapes was investigated with a fiber continuum light source. We found that bleaching rate differences could be largely explained by the second harmonic component content of the pulses and presented a model that agrees reasonably well with the experimental results. The demonstration that shaped pulses can be superior to TL ones, as reported by Kawano et al. [19] appears to be consistent with our results. Their frequency resolved optical gating (FROG) data shows the pulse to have its strongest second harmonic components shifted from 408 to 418 nm (816 to 836 nm fundamental).

In bleaching rate measurements with narrow bandwidth pulses, shorter TL pulses were found to be superior to longer dispersion-broadened or reduced bandwidth pulses, consistent with results previously reported for other fluorophores [17, 18]. While these effects are smaller than the effect of changing the center pulse wavelength there is a useful benefit to two-photon microscopy by dispersion compensation and shortening the excitation pulse. Compensating the $\sim 10000 \text{ fs}^2$ of dispersion in our microscope resulted in a 20 % decrease in bleach rate with $\approx 165 \text{ fs}$ TL pulses. These effects were not apparent with the shorter pulses due to noise caused by the instability of the fiber source and the large changes in bleaching caused by differences in the excitation wavelength.

Over a 800 nm to 950 nm wavelength range the bleach rate was found to be proportional to the $\approx 1.7^{\text{th}}$ power of the excitation rate, or the $\approx 3.4^{\text{th}}$ power of the excitation power. This super-quadratic power dependence implies that multi-photon or multiple excitation events have a role in the bleaching process. Three-photon excitation events are however not expected to be influencing the bleaching as

the shorter pulse lengths would then be expected to have stronger bleaching contrary to the pulse shaper results presented. Bleaching events may represent a two-photon event followed by a two-photon or one photon absorption while the fluorophore is still in an excited or triplet state [32].

A key direction for future work is to establish the pulse length at which the excitation wavelength effects override the bleaching improvement due to reduced pulse length. To improve these results the fiber light source should be modified to improve its stability, possibly by active alignment of the fiber. A pulse shaper using a prism as the dispersive element [33] to give more than the current 25 % transmission or a higher power fiber source would allow a wider range of pulse widths and shapes to be measured with equal brightness. Pulses varying from 15 fs TL (broadband) to 200 fs TL (narrow band) could then be directly compared with the same system and the optimum pulse properties to minimize bleaching could then be established.

For investigators using two-photon microscopy with eGFP we can make the following recommendations: The excitation wavelength has a strong effect on the bleach rate and it is highly desirable to use longer wavelengths, near the 925 nm eGFP excitation peak. An order of magnitude reduction in bleach rate is available by shifting from 800 to 925 nm at a constant excitation rate. Dispersion compensation and the use of shorter excitation pulses can also provide a smaller but still useful improvement in the bleach rate. A 25 % improvement in fluorescence yield was achieved by removing the $\sim 10000 \text{ fs}^2$ dispersion of our microscope and reducing the pulse length from 275 fs to 165 fs.

Acknowledgments The authors would like to thank Drs. Z. Gryczynski and I. Gryczynski of the University of North Texas Health Science Center for making their Mai Tai femtosecond pulse laser available, which enabled completion of this work.

References

1. Denk W, Strickler JH, Webb WW (1990) Two-photon laser scanning fluorescence microscopy. *Science* 248(4951):73–76
2. Helmchen F, Denk W (2005) Deep tissue two-photon microscopy. *Nat Methods* 2:932–940
3. Kobat D, Horton NG, Xu C (2011) In vivo two-photon microscopy to 1.6-mm depth in mouse cortex. *J Biomed Opt* 16(10):106014
4. Xu C, Webb WW (1996) Measurement of two-photon excitation cross sections of molecular fluorophores with data from 690 to 1050 nm. *J Opt Soc Am B* 13(3):481–491
5. Giepmans BNG, Adams SR, Ellisman MH, Tsien RY (2006) The fluorescent toolbox for assessing protein location and function. *Science* 312(217):217–224
6. Shaner NC, Steinbach PA, Tsien RY (2005) A guide to choosing fluorescent proteins. *Nat Methods* 2(12):905–909
7. Blab GA, Lommerse PHM, Cognet L, Harms GS, Schmidt T (2001) Two-photon excitation action cross-sections of the autofluorescent proteins. *Chem Phys Lett* 350:71–77

8. Drobizhev M, Makarov NS, Tillo SE, Hughes TE, Rebane A (2011) Two-photon absorption properties of fluorescent proteins. *Nat Methods* 8(5):393–399
9. Heim R, Tsien RY (1996) Engineering green fluorescent protein for improved brightness, longer wavelengths and fluorescence resonance energy transfer. *Curr Biol* 6:178–182
10. Petrášek Z, Schwille P (2008) Photobleaching in two-photon scanning fluorescence correlation spectroscopy. *ChemPhysChem* 9:147–158
11. Levin MK, Carson JH (2004) Fluorescence correlation spectroscopy and quantitative cell biology. *Differentiation* 72:1–10
12. Brown CM, Dalal RB, Hebert B, Digman MA, Horwitz AR, Gratton E (2007) Raster image correlation spectroscopy (rics) for measuring fast protein dynamics and concentrations with a commercial laser scanning confocal microscope. *J Microsc* 229(1):78–91
13. Dittrich PS, Schwille P (2001) Photobleaching and stabilization of fluorophores used for single-molecule analysis with one- and two-photon excitation. *Appl Phys B* 73:829–837
14. Herz J, Siffrin V, Hauser AE, Brandt AU, Leuenberger T, Radbruch H, Zipp F, Niesner RA (2010) Expanding two-photon intravital microscopy to the infrared by means of optical parametric oscillator. *Biophys J* 98:715–723
15. Donnert G, Eggeling C, Hell SW (2007) Major signal increase in fluorescence microscopy through dark-state relaxation. *Nat Methods* 4(1):81–86
16. Ji N, Magee JC, Betzig E (2008) High-speed, low-photodamage nonlinear imaging using passive pulse splitters. *Nat Methods* 5(2):197–202
17. Xi P, Andegeko Y, Weisel LR, Lozovoy VV, Dantus M (2008) Greater signal, increased depth, and less photobleaching in two-photon microscopy with 10 fs pulses. *Opt Commun* 281:1841–1849
18. Field JJ, Carriles R, Sheetz KE, Chandler EV, Hoover EE, Tillo SE, Hughes TE, Sylvester AW, Kleinfeld D, Squier JA (2010) Optimizing the fluorescent yield in two-photon laser scanning microscopy with dispersion compensation. *Opt Express* 18(13):13661–13672
19. Kawano H, Nabekawa Y, Suda A, Oishi Y, Mizuno H, Miyawaki A, Midorikawa K (2003) Attenuation of photobleaching in two-photon excitation fluorescence from green fluorescent protein with shaped excitation pulses. *Biochem Biophys Res Commun* 311:592–596
20. Dudley JM, Genty G, Coen S (2006) Supercontinuum generation in photonic crystal fiber. *Rev Mod Phys* 78:1135–1184
21. Tu H, Liu Y, Lægsgaard J, Sharma U, Siegel M, Kopf D, Boppart SA (2010) Scalar generalized nonlinear schrödinger equation-quantified continuum generation in an all-normal dispersion photonic crystal fiber for broadband coherent optical sources. *Opt Express* 18(26):27872–27884
22. Hooper LE, Mosley PJ, Muir AC, Yu F, Mangan BJ, Wadsworth W, Knight JC, Dudley JM (2011) Coherent widely tunable source of sub-picosecond pulses using all-normal dispersion fiber supercontinuum. In: Workshop on fibre and optical passive components
23. Baltuška A, Wei Z, Pshenichnikov MS, Wiersma DA (1997) Optical pulse compression to 5 fs at a 1-mhz repetition rate. *Opt Lett* 22(2):102–104
24. Cheng Z, Krausz F, Spielmann C (2002) Compression of 2 mj kilohertz laser pulses to 17.5 fs by pairing double-prism compressor: analysis and performance. *Opt Commun* 201:145–155
25. Walowicz KA, Pastirk I, Lozovoy VV, Dantus M (2002) Multiphoton intrapulse interference. 1. control of multiphoton processes in condensed phases. *J Phys Chem A* 106(41):9369–9373
26. Xu B, Gunn JM, Cruz JMD, Lozovoy VV, Dantus M (2006) Quantitative investigation of the multiphoton intrapulse interference phase scan method for simultaneous phase measurement and compensation of femtosecond laser pulses. *J Opt Soc Am B* 23(4):750–759
27. Brenner MH, Cai D, Swanson JA, Ogilvie JP (2013) Two-photon imaging of multiple fluorescent proteins by phase-shaping and linear unmixing with a single broadband laser. *Opt Express* 21(14):17256–17264
28. Liu Y, Tu H, Benalcazar WA, Chaney EJ, Boppart SA (2012) Multimodal nonlinear microscopy by shaping a fiber supercontinuum from 900 to 1160 nm. *IEEE J Sel Top Quantum Electron* 18(3):1209–1214
29. Xu B, Gunn JM, Cruz JMD, Lozovoy VV, Dantus M (2006) Quantitative investigation of the multiphoton intrapulse interference phase scan method for simultaneous phase measurement and compensation of femtosecond laser pulses. *J Opt Soc Am B* 23(4):750–759
30. Comstock M, Lozovoy VV, Pastirk I, Dantus M (2004) Multiphoton intrapulse interference 6; binary phase shaping. *Opt Express* 12(6):1061–1066
31. Lozovoy VV, Pastirk I, Walowicz KA, Dantus M (2003) Multiphoton intrapulse interference. ii. control of two- and three-photon laser induced fluorescence with shaped pulses. *J Chem Phys* 118(7):3187–3196
32. Patterson GH, Piston DW (2000) Photobleaching in two-photon excitation microscopy. *Biophys J* 78:2159–2162
33. Field JJ, Planchon TA, Amir W, Durfee CG, Squier JA (2008) Characterization of a high efficiency, ultrashort pulse shaper incorporating a reflective 4096-element spatial light modulator. *Opt Commun* 278(2):368–376